Electronic Supplementary Information

Electrochemical Integration of amorphous NiFe-(oxy)hydroxides on Surface-Activated Carbon Fibers for High-Efficient Oxygen Evolution in Alkaline Anion Exchange Membrane Water Electrolysis

Pandiarajan Thangavel[a*], Guntae Kim[b*], and Kwang S. Kim[a*]

[a]*Center for Superfunctional Materials, Department of Chemistry, Ulsan National Institute of Science and Technology (UNIST), 50 UNIST-gil, Ulsan 44919, Korea.*

[b]*School of Energy & Chemical Engineering, Ulsan National Institute of Science and Technology (UNIST), 50 UNIST-gil, Ulsan 44919, Korea.*

**Email:pandiarajan@unist.ac.kr;kimks@unist.ac.kr; gtkim@unist.ac.kr*

Materials and Methods:

Materials:

Toray carbon papers(TGP-H-060) were purchased from Alfa Aesar. Analytical grade, Nickel Sulfate heptahydrate ($NiSO_4.6H_2O$), Ferrous Sulfate heptahydrate ($FeSO_4.7H_2O$), Sodium n-Dodecyl Sulfate (SDS) ($CH_3 (CH_2)_{11}OSO_3Na$), and Potassium Hydroxide (KOH) were purchased from Sigma-Aldrich and used without any further purification. Electrolytes used for the electrochemical studies and electrodeposition process were prepared by Milli Q water (resistivity 18.2 MΩ cm).

Methods:

Pre-treatment of carbon fiber paper (CFP): Prior to the electrodeposition process, carbon fiber papers (2 cm x 2 cm) were ultrasonically cleaned for 10 minutes with conc.HNO_3, ethanol, and milli-q water, respectively.

Surface activation through N_2-Plasma Etching: The as-obtained CFP was further treated under N_2 plasma for 2-minutes,3-minutes, and 5-minutes, respectively, on both sides before the electrodeposition process, using FEMTO science cograde multi generator plasma system (RF generator 300W, 20-1000 kHz).

Synthesis of a-NiFeOOH/N-CFP : The electrolyte bath composed of 0.5 M $NiSO_4.7H_2O$, 0.05 M $FeSO_4.7H_2O$, and 0.5 M SDS. Electrolyte solution purged with N_2 for 20-30 minutes prior to the electrodeposition process to avoid the Fe^{2+} oxidation. The co-electrodeposition was carried out in a standard three electrode system using Pt foil (2cm × 2cm), pre-treated CFP and Ag/AgCl (3.0 M NaCl) as counter electrode, working electrode, and reference electrode, respectively. A constant potential of -1.3V vs. Ag/AgCl was applied for 300 s to deposit NiFe on CFP. After electrodeposition, the working

electrode was carefully removed from the system and rinsed several times with ethanol and water, finally dried at 60 ℃. The catalyst loading amount on CFP was determined by the weight difference before and after the electrodeposition process. Actual catalyst loading after electrodeposition was ~0.091 mg cm^{-2}.

For comparison studies a-NiFeOOH/CFP also prepared using CFP without surface activation.

Synthesis of NiFeLDH/Nickel Foam (NF): Electrodeposition of NiFeLDH ON NF was prepared according to the previous report of Zhenhua Li et.al.[1] The electrolyte bath for the electrosynthesis of NiFe-LDH consists of $Ni(NO_3)_2 \cdot 6H_2O$ (0.15 M) and $Fe(SO_4)_2 \cdot 7H_2O$ (0.15 M) in 50 mL of distilled water with a continuous N_2 flow to avoid Fe^{2+} oxidation. Pre-treated NF and Pt plate (2cm*2cm) working and counter electrode, respectively. The electrodeposition was carried out at a potential of -1.0 V vs. SCE. The resulting NiFe-LDH/NF electrode was carefully removed from the electrolyte bath and rinsed thoroughly with ultra-pure water.

Synthesis of $MoNi_4/MoO_2$ cuboids on nickel foam electrodes: $NiMoO_4$ cuboids on nickel foam was synthesized reported by the hydrothermal method reported in the literature.[2] The catalysts loading weight of the formed $MoNi_4$/ MoO_2 nanoparticles on the nickel foam was ~ 42.3 mg cm^2.

Preparation of IrO_2 /CFP working electrode: 5.0 mg of each catalyst was dispersed in 310 µL of isopropyl alcohol (IPA), 110 µL of deionised water and 80 µL of alkaline anion exchange membrane (AAEM) binder solution and sonicated for 30-60 minutes to form a homogeneous ink. Then, the catalyst ink was loaded onto the pre-treated CFP (catalyst loading of 1mg cm^{-2}) and dried at 60 ^oC.

Preparation of 20 % Pt/C/NF Cathode: Same with the above preparation of IrO_2/CFP working electrode except that pre-treated CFP was replaced by pre-treated NF.

Physical Characterisation: X-ray diffraction (XRD) measurements were carried out using an X-ray diffractometer (Model D8 Advance, Bucker) with a Cu-Kα1 X-ray (λ = 0.15418 Å) source. Raman analyses of the electrodes were performed using a Senterra Raman Scope system with 532 nm wavelength incident laser light and 20 mW power. The chemical states and the composition of the electrodes were investigated using energy-X-ray photoelectron spectroscopy XPS (K-alpha, Thermosphere). The surface morphologies of the electrodes were analysed by high-resolution transmission electron microscopy HRTEM (JEM-2100F, JEOL) as well as Nova NanoSEM (Nano230 FE-SEM) with EDS. The weight percentages of elements in the catalyst were determined using ICP-MS (Perkin Elmer, ELAN DRC-II) and EA (Flash 2000, Thermo Fisher). Phoenix 300 system was used to measure the surface wettability of the electrodes.

Electrochemical characterisation: Electrochemical measurements were performed in a standard three-electrode system, using a VMP3 multi-channel Potentiostat (Bio-Logic Science) and VersaSTAT-3 Potentiostat/ Galvanostat (Princeton Applied Research) at room temperature (25 ± 1 ^{o}C). A Pt foil electrode (2cm × 2cm) and Hg/HgO (1 M NaOH) electrode were used as counter and reference electrode, respectively. All the potentials were reported versus RHE and corrected for solution resistance (R_{sol}) unless otherwise stated.

Reference electrode calibration and RHE Conversion:

The calibration of Hg/HgO electrode was carried out in a standard three-electrode system using Pt wires as the working and counter electrodes, and the Hg/HgO as the reference electrode. 1 M KOH solution (pH =13.6) was saturated with high purity H_2 and used as electrolyte. Then, linear

scanning voltammetry (LSV) was performed at a slow scan rate of 1.0 mV s^{-1} **(Fig. S1)**, and the potential at which the current crossed zero is taken as the thermodynamic potential for the hydrogen electrode reactions. All potentials were measured with respect to Hg/HgO reference electrode and converted to the reversible hydrogen electrode (RHE) scale, using the following equation:

$$E_{RHE} = E_{Hg/HgO} + 0.098V + (0.059 \times pH)$$

All electrochemical experiments were performed in oxygen (O_2) gas saturated 1 M aqueous KOH solution to ensure the O_2/H_2O equilibrium potential 1.23 V. Before the electrochemical measurements, the electrodes were electrochemically stabilized through CV cycling between 1.1-1.6 V (vs RHE) with a scan rate of 50 mV s^{-1}. Cyclic voltammograms and linear sweep voltammetry (LSV) measurements were performed with a scan rate of 1 mV s^{-1} . steady state Tafel plots were measured through chronoamperometric method by applying different potentials for at-least 30 minutes. The Nyquist plots for the samples were measured in the frequency range 100 kHz to 10 mHz, 1.5 V versus RHE, with an AC voltage amplitude of 10 mV. Impedance data were fitted with z-fit (Bio-logic) software. The multistep chronopotentiometric measurements were performed in 1.0 M aqueous KOH solution from 10 to 500 mA cm^{-2}. The chronopotentiometry data was measured by applying a constant current density of 100 $mAcm^{-2}$.

Calculation Methods

i. Electrochemical Active Surface Area (ECSA): Electrochemical active surface (ECSA) of the electrodes was estimated by the double layer capacitance (C_{dl}) in the non-Faradic region from static CV measurements.[3,4] A potential range of 0.02-0.1(V vs. Hg/HgO) was applied to measure the

charge discharge current via CV at different scan rates ranging from 10, 20, 30, 40 and 50 mV s^{-1}**.** Then, plotting the double layer charging current vs. scan rate yields a linear slope, which is equivalent to the twice of C_{dl}. ECSA was obtained by dividing the C_{dl} with the specific capacitance (Cs) of the electrode material. For flat surface electrodes the specific capacitance is 0.04 mF cm^{-2} .

$$ECSA = \frac{Double\ layer\ capacitance(C_{dl})(mF)}{Specific\ capacitance(Cs)(mFcm^{-2})} \times S'(cm^{-2}) \quad \rightarrow S1$$

ii. Roughness Factor :

$$RF = \frac{ECSA\ \ (cm^{-2})}{geometrical\ surface\ area\ of\ electrode\ (cm^{-2})} \quad \rightarrow S2$$

iii. Mass Activity (jm, A.g^{-1}):

$$j_m = \frac{j_{geo}}{m} \quad \rightarrow S3$$

where,

j_{geo} = measured current density (A cm^{-2})

m = catalyst loading (g)

iv. Turn-over frequency (TOF): The TOF (lower bound) of the electrode materials was calculated based on the surface concentration of the active sites in the catalyst material reported in the literature.[3,4]

$$TOF(S^{-1}) = \frac{(J \times N_A)}{(4 \times F \times \Gamma)} \quad \rightarrow S5$$

where,

J=current density (A cm^{-2})

N_A=Avogadro Number (6.023×10^{23})

F = Faraday constant (96,485 C mol^{-1})

Γ = surface concentration of active sites or number of participating atoms in the catalyst material

v. Faradaic Efficiency (Water Displacement Method):

The Faradic efficiency was calculated from the total charge passed through the system at corresponding time intervals using Faraday's law, based on the equation reported in the literatures.[5, 6]

Faradic efficiency=(nF×m)/Q,

where F = Faraday's constant (96,485.33 A s mol^{-1}), n = 4 for OER,

m = moles of gas produced,

Q = amount of charge passed.

Conventional Electrolyser Fabrication for practical water splitting :

As-prepared a-NiFeOOH/N-CFP (anode) and Pt-coated Ti mesh (cathode) in a simple H-type electrochemical cell (Pine Instruments) separated by a fine-frit was used as a conventional electrolyser. 1 M aqueous KOH was used a electrolyte, and prior to electrochemical measurements, the anodic and cathodic compartments were saturated with the O_2 and H_2 gas, respectively. All polarization curves were recorded with a scan rate of 1 mV s^{-1} at room temperature and corrected for the solution resistance. Commercial Pt/C and IrO_2 electrolysers were also fabricated and tested

under similar condition for the comparison. The chronoamperometric data was measured by applying a constant potential of 1.5 V.

Alkaline Anion Exchange Membrane Water Electrolysis (AAEMWE):

Membrane (FAA-3-50) Pretreatment: The alkaline anion exchange membrane was purchased from the fuel cell store, delivered in bromide form and dry state. For alkaline applications, the membrane was converted into hydroxyl form. So, the membrane was kept in an aqueous solution of 0.5 M KOH for 24 h at 25 ° C, and then for 1 h in deionized water. To avoid CO_2 contamination, the pre-treated membrane should be stored under humidified and CO_2 free condition.

Membrane Electrode Assembly(MEA) Fabrication :

Fabrication of MEA using Catalysts Coated on the Substrate (CCS) Method [7]

To fabricate MEA, the Pre-treated AAEM was sandwiched between the a-NiFeOOH/N-CFP anode and $MoNi_4/MoO_2$/NF cathode, followed by hot-pressed for 180 s. Then it was mounted into home-made electrolyser hardware with Ti water flow-field and stainless-steel end plate. Platinized Titanium (PtTi) Screens (0.002 inch) are used as a gas diffusion layer. The working area of the electrolyzer is 4 cm^2. For comparison studies, the commercial MEA was fabricated using IrO_2 and 20% Pt/C on the NF with a maximum catalyst loading of 2.5 mg cm^{-2} and 5mg cm^{-2}, respectively.

Single Cell performance Analysis

All electrochemical experiments were performed using ultra-pure water as an electrolyte at 50 ^oC under ambient pressure. The electrolyte was fed into the cathode side and recirculated with a water circulator pump. Stability studies were performed by applying a cell voltage of 2.0 V, and the whole set-up was periodically disturbed for EIS measurements. The steady state polarization

curves were measured by applying constant potential for at least 30 minutes at different cell potential ranging from 1.2 to 2.2 V. The experiments were repeated 3-4 times at each potential, and the average value obtained from repeated experiments used for plotting the I-V curve.

Solar to Hydrogen Studies:

For unbiassed water splitting demonstration, conventional electrolyser and AAEMWE were directly connected to the commercial photovoltaics and the water splitting experiments were performed in the presence of direct sunlight.[8] The electrolysis current was measured with regular time interval as a function of potential in the day sunlight using commercial photovoltaics. The measured current density was normalized to area of the working electrode.

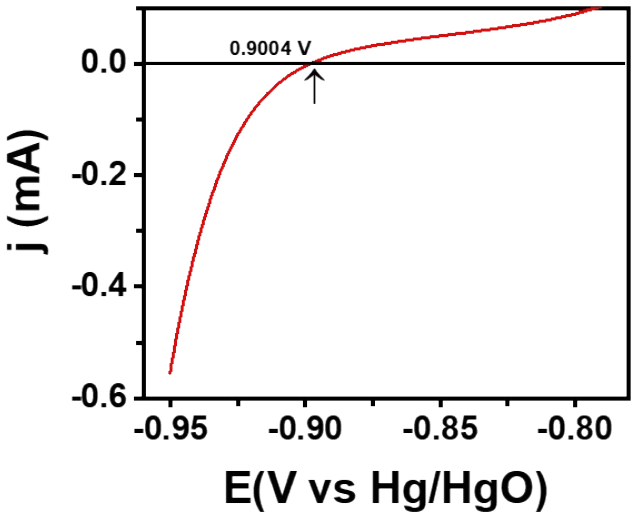

Fig. S1 RHE calibration curve for the Hg/HgO reference electrode.

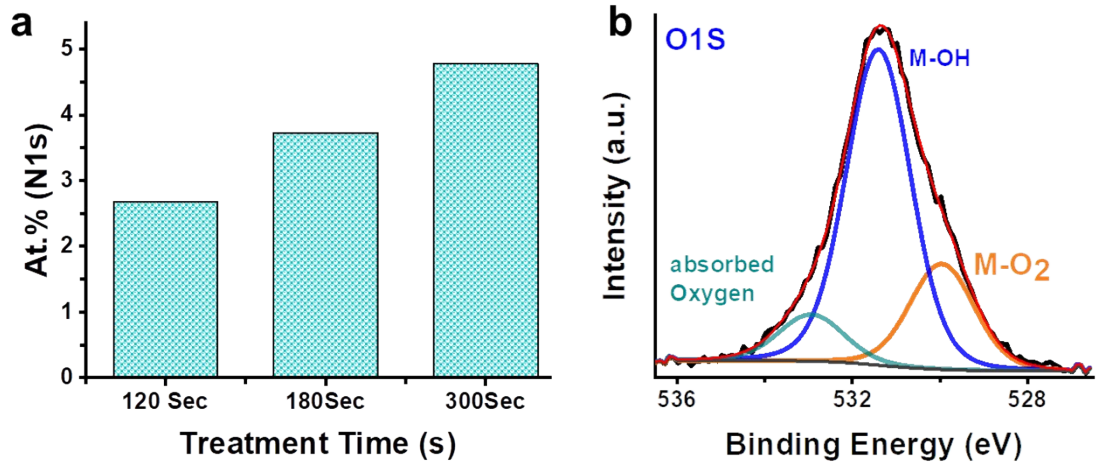

Fig. S2 High-Resolution XPS spectra of a-NiFeOOH /N-CFP. (a) The at. % of N 1s as a function of time calculated from XPS analysis. (b) O1s spectra.

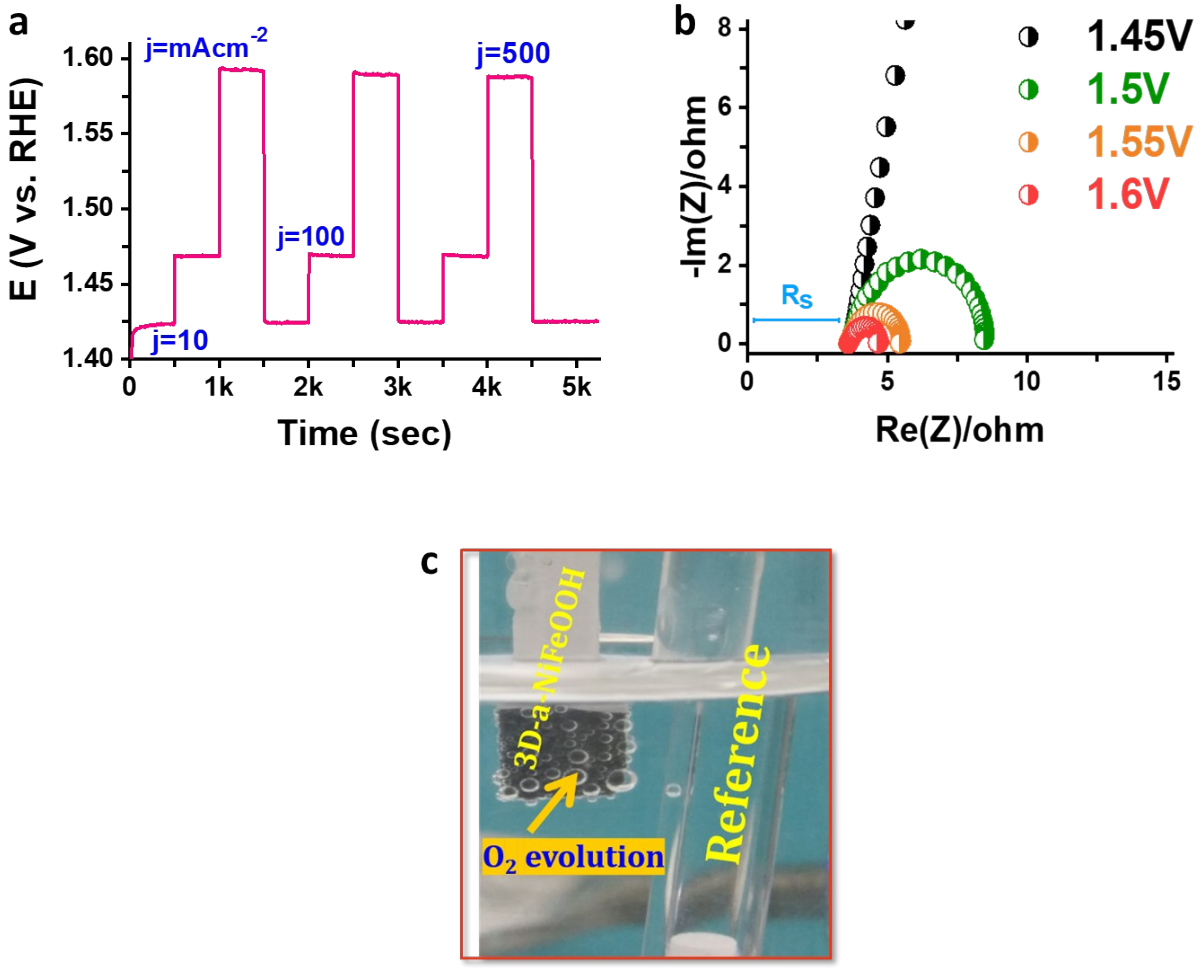

Fig. S3 (a) Multi-step chronopotentiometric curve of a-NiFeOOH/N-CFP electrode at varying current densities without *iR*-compensation. (b) Impedance spectra of the a-NiFeOOH/N-CFP electrode as a function of various applied potentials (1.45-1.6V). (c) Photograph of oxygen evolution (bubbles) at the electrode surface during the OER tests through LSV.

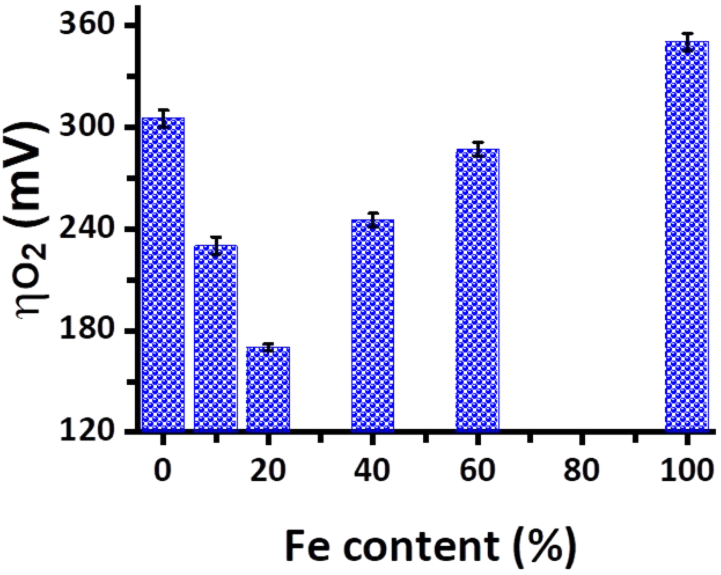

Fig. S4 Effect of Fe concentration on the OER activity of a-NiFeOOH/N-CFP.

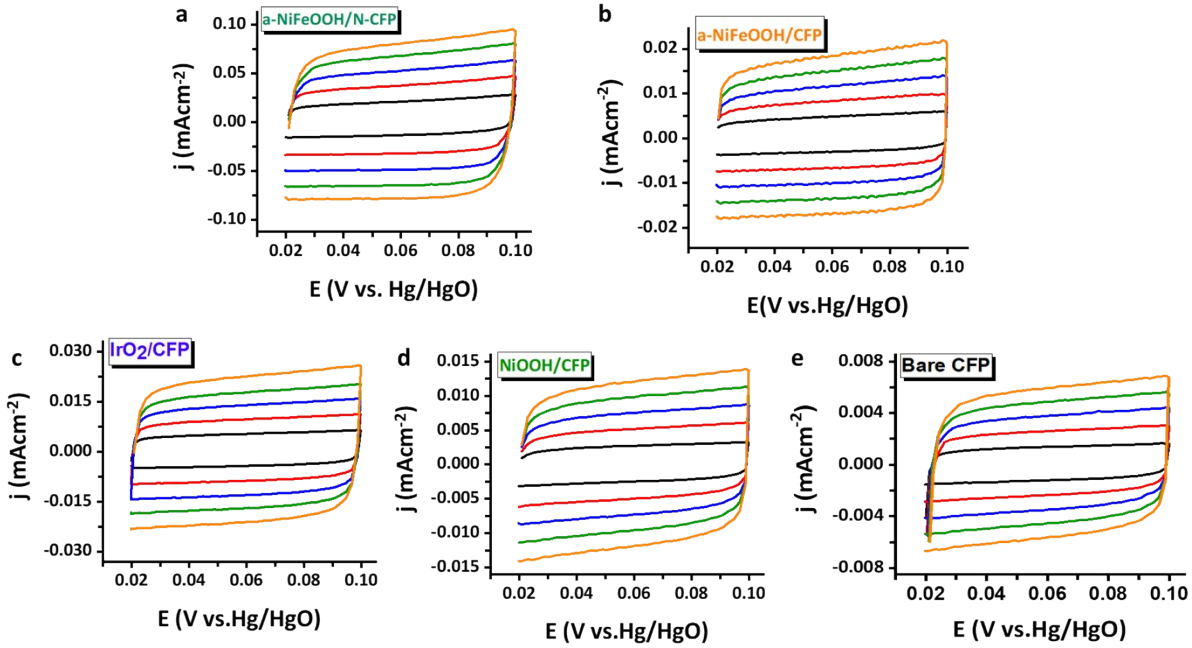

Fig. S5 The capacitive currents at the potential window of 0.02 to 0.10 (V vs. Hg/HgO) as a function of different scan rates (10,20,30,40 and 50 mV) for (a) a-NiFeOOH/N-CFP, (b) a-NiFeOOH/CFP, (c) IrO_2/CFP, (d)NiOOH and (e) bare CFP.

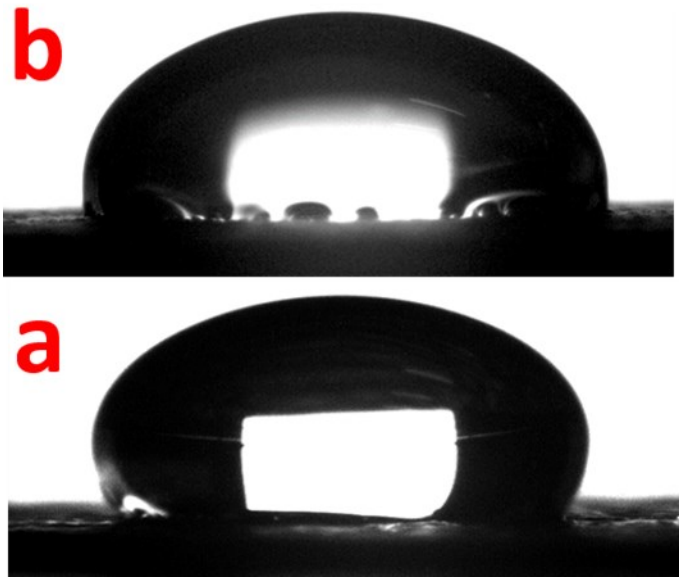

Fig. S6 Contact angle measurements for (a) a-NiFeOOH/N-CFP and (b) bare CFP electrode.

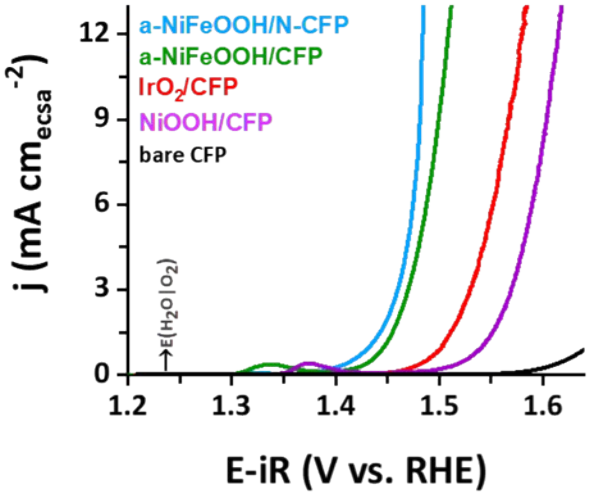

Fig. S7 ECSA normalized LSV curves of the electrodes in 1 M KOH solution at a scan rate of 1 mV s^{-1}.

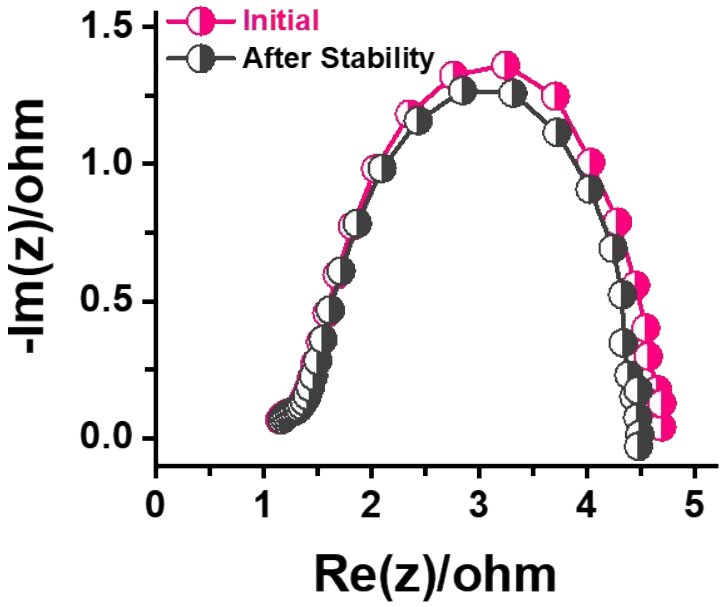

Fig. S8 Impedance spectra of the a-NiFeOOH/N-CFP electrode before and after stability studies at applied potential of 1.5 V.

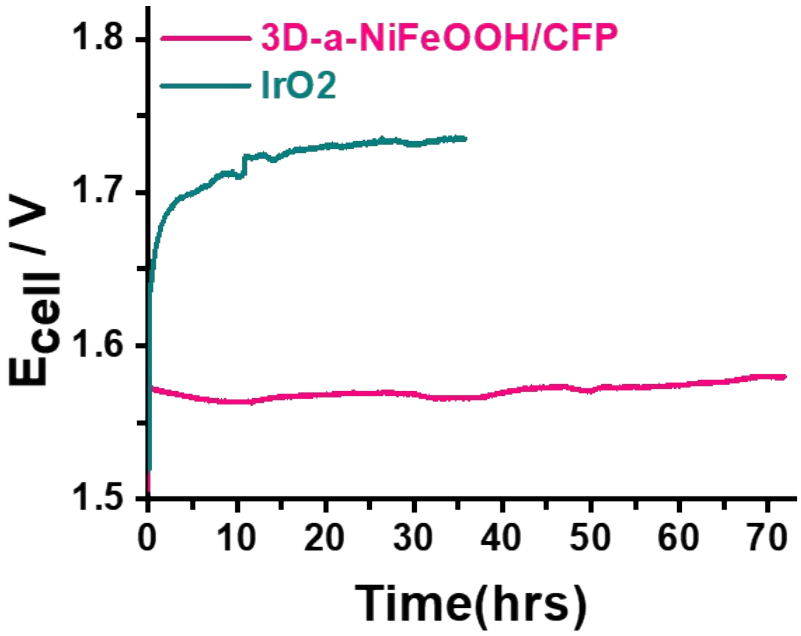

Fig. S9 Chronopotentiometry curves of a-NiFeOOH/N-CFP and IrO_2 based electrolyzer at a constant current density of 100 mA cm^{-2}.

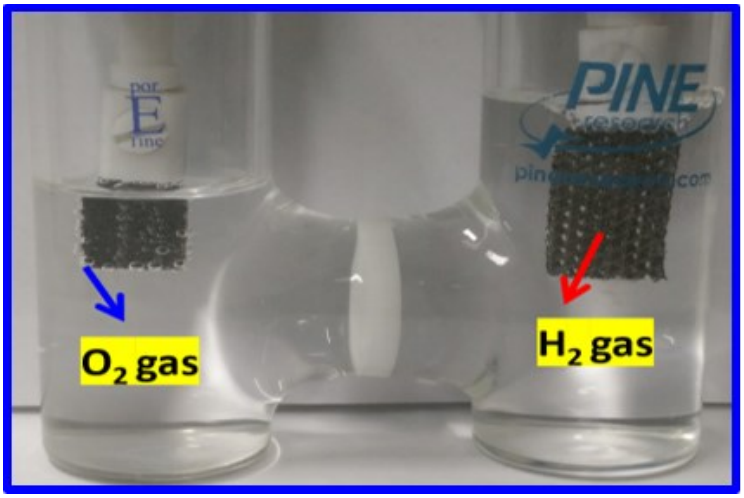

Fig. S10 Digital photograph shows the O_2 and H_2 gas evolution at the electrode surface of conventional electrolyser.

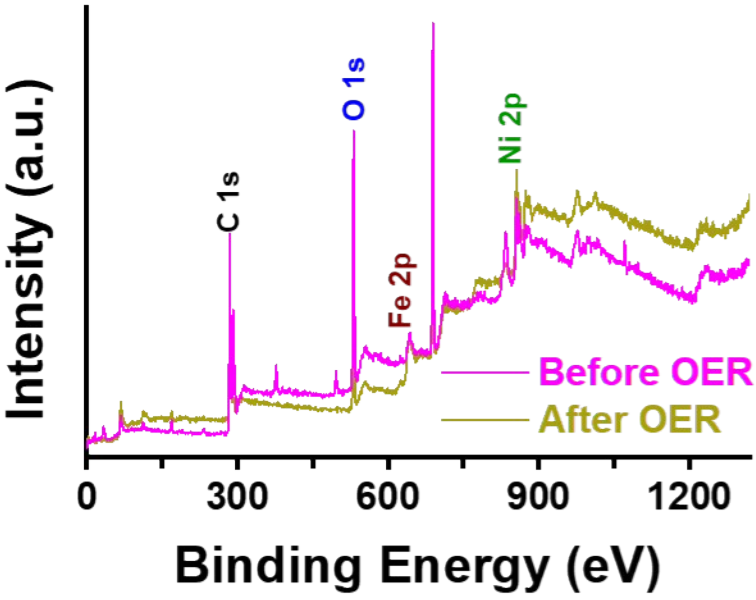

Fig. S11 XPS spectra of the a-NiFeOOH/N-CFP electrode before and after stability studies.

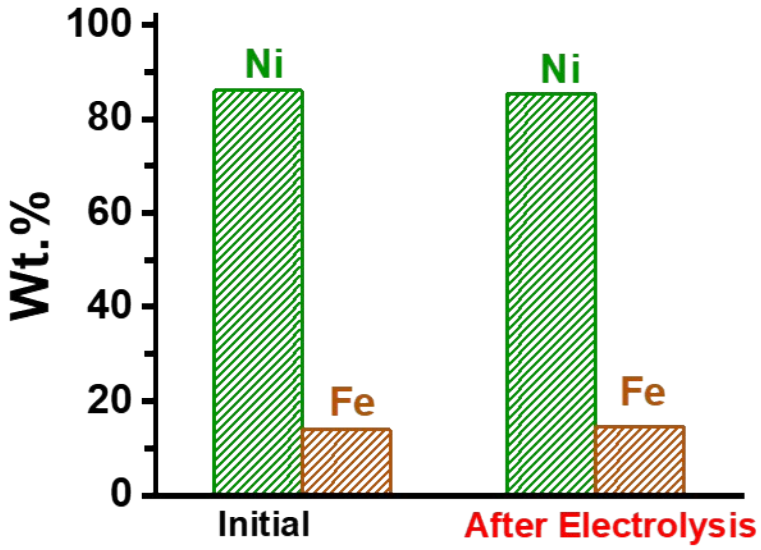

Fig. S12 ICP-MS analysis of the a-NiFeOOH/N-CFP electrode before and after stability studies.

Table S1 Comparison of catalytic performance of a-$Ni_{0.86}Fe_{0.14}OOH$/N-CFP with previously reported state-of-the art Ni, NiFe based catalyst and IrO_2 nanoparticles.

Catalysts	Mass Loading (mg cm^{-2})	η@10 mA cm^{-2} (mV)	Reference
a-$Ni_{0.86}Fe_{0.14}OOH$/N-CFP	**0.091**	**170**	**This Work**
IrO_2/CFP	**1.0**	**290**	**This Work**
Ni-P-B/Paper	6.51	263	*Energy Environ. Sci.,**2020**,Advance Article, 10.1039/C9EE00839J*
LiCoBPO/NF	3.0	293	*Energy Environ. Sci., **2019**,12, 988-999.*
$Ni_{11}(HPO_3)_8(OH)_6$/NF	3.0	232	*Energy Environ. Sci., **2018,**11, 1287-1298.*
CS-NiFeCu	10.2	180	*Nat. Commun., **2018,** 9, 381.*
Fe-Ni@NC-CNTs	0.5	274	*Angew. Chem. Int. Ed., **2018,** 57,8921-8926.*
$Na_{0.08}Ni_{0.9}Fe_{0.1}O_2$	0.13	260	*Energy. Environ. Sci., **2017,** 10, 121-128.*
CoNi(20:1)-P-NS@NF	0.15	209	*Energy & Environ., Sci. **2017**, 10, 893.*
NiFeOOH/CNT	0.28	278	*RSC Adv., **2016**,6, 74536-74544.*
In situ-NiFe–OOH	NA	190	*Mater. Chem. Front., **2017**,1, 2541-2546.*
Oxygen vacancy rich NiFeOOH	NA	~230	*ACS Energy Lett. **2018**, 3, 7, 1515–1520.*
NiD-PCC	8.0	360	*Energy Environ. Sci., **2016,**9, 3411-3416.*
Ni–P nanoplates	0.2	300	*Energy Environ. Sci., **2016**, 9,1246—1250.*
N-NiFeOOH	NA	243	*J. Catal. **2020**, 389, 375– 381.*
$Ni_{60}Fe_{30}Mn_{10}$	19.0	200	*Energy Environ. Sci., **2016**, 9, 540–549.*
FeNi@NC	0.32	280	*Energy Environ. Sci., **2016**, 9,123—129.*
NiV-LDH	0.143	320	*Nat.Commun., **2016**, 7, 11981.*
Gelled FeCoW-OOH	0.39	191	*Science **2016**, 352, 27, 333–337.*
NiFe-LDH (Exfoliated 2-D Nanosheets)	0.25	300	*ACS Nano **2015**, 9, 1977-1984.*

NF- Nickel Foam; CFP- carbon Fiber Paper; LDH- layered double hydroxides ; PCC- Porous Carbon Cloth

Table S2 Comparison of electro kinetic parameters of the catalytic materials measured in 1 M aqueous KOH solution at 25 ^{o}C.

Catalysts	**R_{CT} (ohm)**	**Tafel slope ($mVdecade^{-1}$)**	**CDL (mF)**	**Roughness Factor**
a-NiFeOOH /N-CFP	3.2	39	1.6	40
a-NiFeOOH /CFP	8.2	42	0.34	8.5
IrO_2	40.12	54	0.26	5.75
Bare CFP	253	130	0.11	2.75

-For NiFeLDH Nickel foam was used as an electrode support hence not included in the list.

Table S3 Physical and chemical data of fumapem® FAA-3 membranes.[9]

fumapem®		**FAA-3-50**
Membrane Type		Anion Exchange Membrane
Appearance/Color		Brown/Transparent
Backing Foil		PET
Reinforcement		None
Counter Ion		Bromide (Br-)
Delivery Form		Dry
Thickness (Dry)	µm	40-50
Cl- / Br- form:		
ion exchange capacity (as chloride form)	meq g-1	2.02
selectivity 0.1 / 0.5 mol/kg KCl at T = 25 °C [a)]	%	95.5
uptake in H_2O at T = 25 °C [b)]	wt %	23
dimensional swelling in H_2O at T = 25 °C [c)]	%	2
specific conductivity in Cl- form [d)]	mS cm^{-1}	7.8
specific area resistance in Cl- form [d)]	Ω cm^2	0.6
OH- form:		
uptake in H_2O at T = 25 °C [e)]	wt %	40
dimensional swelling in H_2O at T = 25 °C [f)]	%	17
specific conductivity in H_2O at T = 25 °C [g)]	mS cm^{-1}	40 - 45
specific area resistance in H_2O at T = 25 °C [g)]	Ω cm^2	0.10 - 0.15

a) determined from membrane potential measurement in a concentration cell.

b) in Br- form, membrane as received, stored in water for 24 h, reference membrane dried over P_2O_5 in vacuo.

c) in Br- form, membrane as received, stored in water for 24 h, reference membrane as received.

d) in Cl^- form in 0.5 M NaCl @ T = 25 °C, measured in standard measuring cell (through-plane).

e) in OH^- form, reference membrane dried over P_2O_5 in vacuo.

f) in OH^- form, reference membrane dried at 25 °C and 50 % r.h.

g) in OH^- form, using a 4-probe cell, in-plane measurement, ac impedance spectroscopy

Please note: The data are not measured directly on the item supplied.

Reference

1. Z. Li, M. Shao, H. An, Z. Wang, S. Xu, M. Wei, D. G. Evans and X. Duan, *Chem. Sci*. **2015**, 6, 6624-6631.
2. J. Zhang, T. Wang, P. Liu, Z. Liao, S. Liu, X. Zhuang, M. Chen, E. Zschech and X. Feng, *Nat. Commun*. **2017**, 8,15437.
3. C. C. L. McCrory, S. H. Jung, J. C. Peters and T. F. Jaramillo, *J. Am. Chem. Soc.* **2013**, 135, 16977-16987.
4. S. Anantharaj, S. R. Ede, K. Karthick, S. S. Sankar, K. Sangeetha, P. E. Karthik and S. Kundu, *Energy Environ. Sci*. **2018**,11,744-771.
5. J. R. Swierk , S. Klaus , L. Trotochaud , A. T. Bell and T. D. Tilley , *J. Phys. Chem. C* **2015**, 119, 19022-19029.
6. M. Zhou, Q. Weng, X. Zhang, X. Wang, Y. Xue, X. Zeng, Y. Bando, D. Golberg, *J. Mater. Chem. A* **2017**, 5, 4335.
7. Y. J. Leng, G. Chen, A. J. Mendoza, T. B. Tighe, M. A. Hickner and C. Y. Wang, *J. Am. Chem. Soc.* **2012**,134,9054-9057.
8. J. Luo, J.-H. Im, M. T. Mayer, M. Schreier, M. K. Nazeeruddin, N.-G. Park, S. D. Tilley, H. J. Fan and M. Grätzel, *Science* **2014**, 345,1593.
9. www.fuelcell store.com.